frontiers | Frontiers in Physiology

TYPE Original Research
PUBLISHED 11 October 2023
DOI 10.3389/fphys.2023.1244060

OPEN ACCESS

EDITED BY
Diana Sofia Madeira,
University of Aveiro, Portugal

REVIEWED BY
Luca Morelli,
University of Aveiro, Portugal
Milan Szabo,
Eötvös Loránd Research Network (ELKH), Hungary
Susana Enríquez,
National Autonomous University of Mexico, Mexico

*CORRESPONDENCE
Audrey McQuagge,
audreymcquagge@gmail.com
Kenneth D. Hoadley,
kdhoadley@ua.edu

RECEIVED 21 June 2023
ACCEPTED 21 September 2023
PUBLISHED 11 October 2023

CITATION
McQuagge A, Pahl KB, Wong S, Melman T, Linn L, Lowry S and Hoadley KD (2023), Cellular traits regulate fluorescence-based light-response phenotypes of coral photosymbionts living *in-hospite*. *Front. Physiol.* 14:1244060. doi: 10.3389/fphys.2023.1244060

Cellular traits regulate fluorescence-based light-response phenotypes of coral photosymbionts living *in-hospite*

Audrey McQuagge[1,2]*, K. Blue Pahl[1,2], Sophie Wong[2,3], Todd Melman[4], Laura Linn[2], Sean Lowry[1,2] and Kenneth D. Hoadley[1,2]*

[1]Department of Biology, University of Alabama, Tuscaloosa, AL, United States, [2]Dauphin Island Sea Lab, Dauphin Island, AL, United States, [3]Department of Environmental Science, University of Virginia, Charlottesville, VA, United States, [4]Reef Systems Coral Farm, New Albany, OH, United States

Diversity across algal family Symbiodiniaceae contributes to the environmental resilience of certain coral species. Chlorophyll-*a* fluorescence measurements are frequently used to determine symbiont health and resilience, but more work is needed to refine these tools and establish how they relate to underlying cellular traits. We examined trait diversity in symbionts from the generas *Cladocopium* and *Durusdinium,* collected from 12 aquacultured coral species. Photophysiological metrics (Φ_{PSII}, σ_{PSII}, ρ, τ_1, τ_2, antenna bed quenching, non-photochemical quenching, and qP) were assessed using a prototype multi-spectral fluorometer over a variable light protocol which yielded a total of 1,360 individual metrics. Photophysiological metrics were then used to establish four unique light-response phenotypic variants. Corals harboring C15 were predominantly found within a single light-response phenotype which clustered separately from all other coral fragments. The majority of *Durusdinium* dominated colonies also formed a separate light-response phenotype which it shared with a few C1 dominated corals. C15 and D1 symbionts appear to differ in which mechanisms they use to dissipate excess light energy. Spectrally dependent variability is also observed across light-response phenotypes that may relate to differences in photopigment utilization. Symbiont cell biochemical and structural traits (atomic C:N:P, cell size, chlorophyll-*a*, neutral lipid content) was also assessed within each sample and differ across light-response phenotypes, linking photophysiological metrics with underlying primary cellular traits. Strong correlations between first- and second-order traits, such as Quantum Yield and cellular N:P content, or light dissipation pathways (qP and NPQ) and C:P underline differences across symbiont types and may also provide a means for using fluorescence-based metrics as biomarkers for certain primary-cellular traits.

KEYWORDS

Symbiodiniaceae, coral photosymbionts, functional traits, chlorophyll-a fluorescence, phenomics

10.3389/fphys.2023.1244060

Introduction

The dinoflagellate algal family Symbiodiniaceae is genetically and phenotypically diverse, having evolved to occupy numerous niches and lifestyles, which include free-living open ocean as well as endosymbiotic roles most notably in stony corals (Muscatine and Hand, 1958; Loeblich and Sherley, 1979; Takabayashi et al., 2012). Within the coral holobiont, Symbiodiniaceae live within coral gastrodermal cells, in which they recycle coral waste products and in turn produce up to 90% of the coral's energy stores through fixed carbon (Yellowlees et al., 2008). Their endosymbiotic relationship with stony corals is complex and dynamic, with differing life histories, coral hosts, and environments giving rise to vast diversity in survival strategies and physiology across the family (Wiedenmann et al., 2012; Pasaribu et al., 2016; Suggett et al., 2017; LaJeunesse et al., 2018). Elevated seawater temperatures above a certain threshold have increased the risk of coral endosymbiont loss (coral bleaching) and its associated sublethal and lethal effects worldwide (Steen and Muscatine, 1987; Hoegh-Guldberg and Smith, 1989; Tchernov et al., 2011). Coral bleaching mitigation and reef restoration relies on improved holistic understanding of the coral holobiont (the coral host and its microbiome, including endosymbiotic algae), to determine what traits underpin resilience under environmental stressors. Association with adaptable and resilient symbiont species is thought to be an important predictor of coral resilience (Suggett et al., 2017), but the underlying phenotypic differences across the family are not fully resolved.

Inherent functional traits of both the algal symbiont and the coral host, as well as their interactive physiology, govern coral bleaching susceptibility which varies across different host-symbiont combinations (Sampayo et al., 2008; Krueger and Gates, 2012; Scheufen et al., 2017). Certain genera of Symbiodiniaceae, such as *Durusdinium* (Clade D) are often linked with higher thermal tolerance across many Caribbean and Pacific coral species where mixed assemblages of photosymbionts are common (LaJeunesse et al., 2003; Baker et al., 2004; Fabricius et al., 2004; Sampayo et al., 2008). For these "symbiont generalist" coral species, dominance by the species *Durusdinium trenchii* is particularly notable among colonies that display higher thermal tolerance. Other coral species only associate with a single symbiont species (specialists), and their responses to thermal stress are often more nuanced and species/environmentally dependent. However, symbiont 'specialist' corals that house *Cladocopium C15* are often more thermally resilient than others, suggesting that *C15* may also be a thermally tolerant symbiont type. What functional traits these two species carry and allow them to be more thermally tolerant than others is an active area of research both for basic and applied fields of coral conservation.

The Symbiodiniaceae family is genetically and phenotypically diverse, but phylogeny alone is not sufficient to explain the broad differences in ecological success that have been observed across the family (Sampayo et al., 2008; Goyen et al., 2017; Suggett et al., 2017; Lewis et al., 2018; Mansour et al., 2018). Relatively recent adaptive radiations among certain genera (Thornhill et al., 2014) driven by variable nutrient and light environments, coral skeletal architecture, and tissue pigments have presumably resulted in diverse functional traits across species, including variability in response to environmental perturbations such as thermal stress (D'Angelo and Wiedenmann, 2014; Sully and van Woesik, 2020; Scheufen et al., 2017; Suggett et al., 2015; Suggett et al., 2017). However, there still exists a gap in knowledge regarding how genomic diversity within this group translates into functional trait differences and phenotypes across species and environments. A better understanding of algal trait variability across the *Symbiodinaceae* family is needed.

Chlorophyll-*a* fluorescence techniques are commonly employed within coral research as a tool for assessing photosynthetic health under high temperature stress (Warner et al., 1999; Rodríguez-Román et al., 2006; Cunning et al., 2021). Indeed, these tools have been a critical component of bleaching response research. Recently, more specialized chlorophyll-a fluorometers known as "single-turnover" instruments capable of measuring changes in fluorescence at 1-µs intervals are increasingly utilized to characterize trait-based differences within and across coral species (Hoadley et al., 2021; Suggett et al., 2022). Incorporation of varying light protocols and multispectral analyses (Szabó et al., 2014; Hoadley et al., 2023) further increases the utility of these tools for assessing nuanced functional trait differences across coral species and/or environmental conditions. Such tools provide the ideal platform for phenomic studies as "high-content" data sets can be easily captured from individual corals and then assessed using machine learning techniques to establish photo-physiological profiles representative of key species and/or underlying cellular traits.

First-order traits, or traits which form the basis of function, are thought to be better determinants of algal survival and success than secondary traits, which arise from the performance of primary traits (Suggett et al., 2017). First-order traits such as allometric scaling (cell size) and nutrient budgeting (atomic Carbon: Nitrogen: Phosphorus ratios) likely regulate second-order traits, such as photoprotection and light utilization strategies (Suggett et al., 2017; McIlroy et al., 2020; Hoadley et al., 2021). However, first order traits are often difficult to measure, requiring destructive and sometimes expensive analytical methodology. In contrast, second order traits, such as light utilization strategies in photosynthetic organisms, are relatively easy to characterize using rapid and non-invasive tools such as chlorophyll-*a* fluorescence (Warner et al., 1999; Suggett et al., 2015; Warner and Suggett, 2016). Because light utilization strategies differ across environmental conditions and species of Symbiodiniaceae, characterizing relationships between such secondary and underlying primary traits could provide useful insight into what drives the observed functional trait differences derived through chlorophyll-*a* fluorescence. By establishing correlations between primary traits and light utilization characteristics, future studies may also be able to infer certain primary trait characteristics via chlorophyll-*a* fluorescence alone.

In this study, we characterized the variable chlorophyll a fluorescence characteristics of six different Symbiodiniaceae species living *in-hospite* among 60 Pacific coral fragments, spanning 12 coral species (*Montipora capricornis*, *Acropora*

yongei, *Montipora digitata*, *Turbinaria reniformis*, *Acropora millepora*, *Acropora humilis*, *Acropora valida*, *Acropora* sp., *Pavona cactus*, *Psammacora contigua*, *Pocillopora damicornis*, *and Cyphastrea chalcidicum*), sourced from the Reef Systems Coral Farm, Inc., in New Albany, Ohio. Prior to isolation of the algal symbionts for characterization of primary traits, we first assessed active chlorophyll-*a* fluorescence metrics using five excitation wavelengths during a time-resolved actinic light protocol designed to test acclimation, relaxation, and light utilization at high and low irradiance (Hoadley et al., 2023). This yielded a total of 1,360 individual metrics which were then used to cluster coral colonies based on similarity of their photophysiological light-response phenotype. Phenotypes were then compared to genetically identified symbiont species and linked to underlying differences in primary traits across light-response phenotypes. Next, a network analysis was used to elucidate specific correlations between our primary and secondary traits. Convergence between algal species and phenotypes provide a useful means for understanding trait-based differences across genetic lineages, along with the underlying cellular traits that regulate them.

Materials and methods

Coral husbandry and environmental conditions

All corals were housed at Reef Systems Coral Farm (New Albany, Ohio). This facility consists of large ~4,000 L raceways (8′ x 4′ x 4′) housed within a greenhouse facility (optically clear plastic roofing with no shade cloth). Smaller indoor tanks (~1,100 L) contain additional corals under LED illumination. All tanks utilize the same artificial seawater (Reef Crystals in RO/DI filtered water) and receive frequent (10%–20%, 1–2 weeks^{-1}) water changes. All tanks contain submersible power heads (Tunze) which circulate water within each system between 50–100 times per hour. Additional overflow pumps exchange water (1–2 times volume of tank hr^{-1}) with external sumps equipped with mechanical (25-micron sieve) and foam fractionation filtration. All coral fragments are mounted on ceramic disks (3 cm) and attached using cyanoacrylate gel (coral glue). Peak irradiance (measured at the same tank depth for each tank) within the outdoor (greenhouse) tanks was 1,050 µmol m^{-2} sec^{-1} (walz, 4pi sensor). Indoor corals were illuminated using LED lighting (Radion Xr30 Pro) on a 10:14 h dark: light cycle with peak irradiance measured at 300 µmol m^{-2} sec^{-1}. Indoor and outdoor corals thus differ both in max irradiance but also in light spectra (natural lighting vs. LED output).

Reef Systems Coral Farm (New Albany, Ohio) houses over 30 different species of coral, with thousands of individual fragments originating from coral colonies that were harvested in Fiji but have been captively grown at the facility for over 10 years. All individual fragments utilized in the study had been fragmented and mounted for at least 1 month prior to use. In order to maximize diversity, we collected three replicate fragments from twenty different coral colonies chosen to include a wide range of life strategies and histories, including both mound and branching species acclimated to greenhouse conditions; *Psammacora contigua* (1 genotype), *A. yongei* (1 genotype), *A. millepora* (1 genotype), *A. humilis* (1 genotype), *A. valida* (1 genotype), *Acropora* species (1 genotype), *T. reniformis* (2 genotypes), *P. cactus* (1 genotype), *M. digitata* (1 genotype), *M. capricornis* (3 genotypes), *C. chalcidicum* (1 genotype), *P. damicornis* (2 genotypes). In addition, indoor acclimated fragments representing species *A. humilis* (1 genotype), *T. reniformis* (1 genotype), and *M. capricornis* (2 genotypes) were also included in our analyses.

Chlorophyll *a* variable fluorescence-based phenotyping protocol

Prior to measurements, each individual coral fragment was dark acclimated for 20–25 min (Suggett et al., 2015). Photophysiological responses to changing light conditions were then measured using a prototype Chlorophyll-*a* fluorometer previously described in Hoadley et al., 2023. Briefly, fluorescence induction curves were produced through excitation with 1.3-µs single turnover flashlets spaced apart by 3.4-µs dark intervals (32 flashlets were utilized under 420, 442, and 458-nm excitation while 40 flashlets were utilized during 505 and 520-nm excitation). Each fluorescence induction curve was followed by a 300 ms relaxation phase consisting of 1.3-µs light flashes spaced apart with exponentially increasing dark periods (starting with 59-*µs*). Fluorescence induction and relaxation curves measured using each excitation wavelength were sequentially repeated five times per measurement timepoint. These photophysiological measurements were repeated 34 times during an 11-min variable actinic light protocol in which corals were exposed to an initial dark period (30s) followed by three different light intensities (300 µmol m^{-2} sec^{-1} for 3.5 min, then 50 µmol m^{-2} sec^{-1} for 1.5 min followed by 600 µmol m^{-2} sec^{-1} for 3.5 min), and a final dark recovery period (~2 min) (Hoadley et al., 2023). Resulting fluorescence data was analyzed using custom R scripts (Hoadley et al., 2023) and according to equations set forth in Kolber et al., 1998 in order to calculate quantum yield of photosystem II (Φ_{PSII}), PSII functional absorption cross-section (σ_{PSII}), reaction center connectivity ρ), non-photochemical quenching (NPQ), antenna bed quenching (ABQ), photochemical quenching (qP), and two time constants for electron transport (τ_1 and τ_2) where τ_1 reflects acceptor-side changes of PSII and τ_2 reflects changes in plastoquinone pool reoxidation (Suggett et al., 2022; Hoadley et al., 2023). However, downstream PQ reoxidation kinetics (τ_2) are typically derived from a multiturnover induction and relaxation flash sequence (Suggett et al., 2022) whereas ours are derived from the second exponential component of a single turnover induction and relaxation flash sequence (τ_2^{ST}).

Endosymbiont isolation

Once chlorophyll-*a* fluorescence-based measurements were complete, a portion of coral tissue was removed using the water-pick method (Johannes and Wiebe, 1970) and filtered seawater (artificial seawater vacuum-filtered, 0.2-micron filter). The resulting tissue-water slurry was homogenized using a hand-held tissue homogenizer (tissue tearer) and then measured using a graduated cylinder. Samples were then centrifuged (8,000 g, 10 min, room

temperature). After centrifugation, the supernatant was removed, and the pellets were resuspended in sterile seawater, vortexed for 30 s and then centrifuged once more to wash the endosymbionts free of the host tissue. Resulting algal pellets were resuspended in 10 mL of sterile seawater.

Flow cytometry (cell size, chlorophyll-*a*, neutral lipid content, and granularity)

One ml aliquots of resuspended algal samples were preserved with glutaraldehyde (0.1% final concentration), incubated in the dark for 20 min, flash frozen in LN_2, and then stored at −80°C for downstream flow cytometry. All samples were analyzed using a Attune NxT (Invitrogen, United States) equipped with a 488-nm (200-mW) laser and a 200-µm nozzle. Glutaraldehyde-fixed samples were re-pelleted using a centrifuge (12,000 g, 5 min), resuspended in 1x filtered PBS, and then filtered through a 50-micron mesh filter to remove residual coral tissue or large cell aggregates. Samples were then diluted 4x with 1x filtered PBS and spiked with 10-µL of 1: 1,000 diluted fluorescent bead stock (Life Technologies 4.0-µm yellow-green 505/515 Fluospheres sulfate). 100-µL per culture was analyzed at a flow rate of 200-µL min^{-1}. For characterization of Symbiodiniaceae cells, data collection was triggered on forward light scatter (FSC), while red (695/40 nm bandpass filter) autofluorescence detected chlorophyll-*a*, and both were utilized to gate the cell and bead populations for bead-normalized FSC, side scatter (SSC) and chlorophyll fluorescence measurements.

For quantification of neutral lipid content, 500-µL of the diluted sample was first stained with 2-µL 5 mM Bodipy 493/503 (Invitrogen, 4,4-Difluoro-1,3,5,7,8-Pentamethyl-4-Bora-3a,4a-Diaza-s-Indacene) and then incubated in the dark at 37°C for 15-min. Stained samples were then run according to the same conditions described above. The Symbiodiniaceae cell population was identified using FSC-height and autofluorescence, and the gated population's green fluorescence was quantified (bandpass filter 530/30).

Total C:N:P content and nutrient analysis

For Carbon and Nitrogen analysis, 2-mL of each resuspended algal sample was filtered through a 13-mm ashed GF/F filter and dried in a 95°C oven for 24-h. Filters were packed into tin capsules, combusted (Costech Instruments 4010 Elemental Combustion System) and analyzed via Elemental Analyzer. Total carbon and nitrogen values were compared to an atropine standard. For particulate organic phosphorus (POP) analysis, 2-mL of each isolate was filtered through a 13-mm ashed GF/F filter and stabilized with a 0.17 M Na_2SO_4 rinse. Filters were placed in muffled scintillation vials with 2-mL aliquots of 0.017 M Na_2SO_4 and evaporated to dryness in a 95°C muffle oven for 24-h. Vials were covered in aluminum foil and baked at 450°C for 2-h, and then were baked with 5-mL 0.2 M HCl at 90°C for 30-min. Samples were diluted with 5-mL ultra-pure water and analyzed using the Skalar SAN + system and compared to an Adenosine Triphosphate standard.

To confirm that corals across different tanks were grown under similar nutrient conditions, 20-mL samples from each husbandry tank were collected and stored at −20°C until analysis, when they were thawed and loaded into the Skalar SAN + system's autosampler. The samples were analyzed for µM nitrate, nitrite, ammonia, and phosphate via continuous flow analysis and according to EPA standard techniques (EPA, 1993a; EPA, 1993b).

DNA sequencing

A 2-mL aliquot of isolated symbiont cells were first pelleted (centrifugation at 10,000 rcf for 5 min) and then stored in 1-mL of DMSO buffer solution (Pettay et al., 2015) at 4°C. DNA was extracted from each sample using the Wizard Genomic DNA Purification Kit (Promega). Quality of DNA samples were assessed on a 1.0 Nanodrop (Thermo Scientific) and all samples had 260/280 and 260/230 values above 1.5. For each sample, PCR was first performed targeting the internal transcribed spacer 2 (ITS2) region using the previously established primer pairs (ITSintfor2: 5′GAATTGCAGA ACTCCGTG-3′, ITS2-reverse: 5′GGGATCCATA TGCTTAAGTT CAGCGGGT-3′) (Sheffield et al., 1989; LaJeunesse, 2002). Resulting amplicons were subjected to a second round of PCR (only eight cycles) using the same primer pairs with adapter sequence (Forward- TCGTCGGCAGCGTCAGAT GTGTATAAGAGACAGGAATTGCAGAACTCCGTG; Reverse-GTCTCGTGGGCTCGGAGATGTGTATAAGAGACAGGGGAT CCATATGCTTAAGTTCAGCGGGT). Adapter sequences are underlined in the above primer sets. All PCR was achieved using Hot Start Taq DNA Polymerase (New England BioLabs, Inc.) under the following settings: denaturation 94.0°C for 30 s, annealing 54.0°C for 35 s, extension 68.0°C for 3 min x 35 cycles (Eight cycles in round two), final extension 68.0°C for 5-min. Samples were then purified using the GeneJET PCR Purification Kit (Thermo Scientific) and visualized on agar gels to confirm results. Amplicons were submitted to the University of Delaware Sequencing and Genotyping Center for library preparation and metagenomic sequencing. Amplicons were dual indexed using the Nextera system and were run as a single library using a paired-end 300 base pair x 2 strategy on an Illumina MiSeq system. Demultiplexed FASTQ sequences were then uploaded to SymPortal for profiling (Hume et al., 2019). Given known high variability in rDNA copy numbers across species and genera (LaJeunesse and Thornhill, 2011) which may hinder translation of data into accurate relative abundances (Davies et al., 2022), absolute abundance ITS2-type profiles were then normalized to rDNA copy numbers according to Saad et al., 2020.

Statistical analyses

All statistical analyses were conducted in R (version 4.1.3). Algal genotypes for each coral sample were derived from SymPortal-generated ITS2 profiles normalized to reflect relative abundance of each symbiont genera. Importantly, known differences in *Cladocopium* and *Durusdinium* ITS2 copy numbers was addressed by normalizing to previously derived rDNA copy ratios of 2119:362 (Saad et al., 2020). The dominant (>70% of ITS2 sequences) symbiont type in each coral fragment (Figure 2B) was then utilized to screen for photophysiological metrics that were significantly different across

algal species using either a one-way ANOVA or Kruskal–Wallis test if data did not meet the assumptions of normality. The resulting dataset was then transformed using Z-scores and then plotted as a heatmap (Figure 2A) with individual coral colonies represented by each column, and photophysiological metrics across rows. A clustering analysis (1,000 bootstrap iterations) was performed using the R packages pvclust (Suzuki and Shimodaira, 2006) and dendextend (Galili, 2015) to cluster individual coral samples by algal phenotype. Clustering analyses were also carried out on heatmap rows and resulting clusters were further analyzed using custom scripts to identify which photophysiological metrics were most important for separating our coral fragments into separate light-response phenotypes.

Full actinic light profiles for identified photophysiological metrics (Figure 2A) were plotted in Figure 3 and a repeated measures linear mixed model with a tukey posthoc (with Bonferroni correction) identified significant differences across algal light-response phenotypes (Supplementary Table S4) using the lmerTest (Kuznetsova et al., 2017) and multicomp (Hothorn et al., 2008) R packages. Spectrally-dependent differences within each photophysiological metric and algal phenotype were similarly assessed (Supplementary Table S3). Significant differences in cellular physiology (cell size, Granularity, Chl *a*, N:P, C:P, and C:N ratios) across phenotypes was also assessed. For each metric, normality was first determined (Shapiro-Wilks). If data were determined to be normal, a One Way ANOVA followed by a Tukey posthoc was performed. For data that did not meet the assumptions of normality, a Kruskal Wallace with Bonferroni correction was performed (Figure 4).

A network analysis was employed to look for significant correlation between photophysiological metrics and primary cellular traits using averaged values across coral species replicates (three species^{--1}). Only correlations with a Pearson value above 0.6 were utilized.

Using the igraph package (Csardi and Nepusz, 2006), specific correlations (Pearson's value of 0.55 or above) between symbiont

TABLE 1 Coral hosts, growth environments, and relative abundances of ITS2 symbiont types determined through SymPortal.

Coral host	Growth environment	Dominant symbiont type (full ITS2 name)	Rel. Abundance	Secondary symbiont type (full ITS2 name)	Rel. Abundance
A. humilis var 1	Outdoor	C3k/C3-C50a-C3dq-C50f-C3ba-C3a	1.00	—	—
A. millepora	Outdoor	C3/C3u-C115-C21ab-C3ge	1.00	—	—
Acropora sp.	Outdoor	C21-C3-C21ag-C21af	1.00	—	—
A. valida	Outdoor	C3z-C3-C3.10-C115-C3an	0.98	C21	0.02
A. yongei	Outdoor	C21-C21ag-C3-C21as	1.00	—	—
C.chalcidium	Outdoor	C1/C3-C1c-C1b-C42.2-C1bh-C1br	1.00	—	—
M.capricornis var 1	Outdoor	C26A-C21	0.98	C1	0.02
M.capricornis var 2	Outdoor	C15-C15he-C15ed-C15cq-C15vl	1.00	—	—
M.capricornis var 3	Outdoor	C15-C15he-C15ed-C15cq-C15vl	1.00	—	—
M.digitata	Outdoor	C15/C15gb-C15vk	1.00	—	—
P. cactus	Outdoor	C1b/C1/C1mm-C3-C1u-C1dg	1.00	—	—
P. contigua	Outdoor	D1-D4-D4c-D1h	0.98	C1ec/C1-C1b-C3	0.02
P. damicornis var 1	Outdoor	D1/D6-D1h-D1kg-D1ke-D1kf-D1kh	0.98	C1d/C1/C42.2/C3-C1b-C3cg-C45c-C115k-C1au-C41p	0.02
P. damicornis var 2	Outdoor	D1/D6-D1h-D1kg-D1ke-D1kf-D1kh	0.84	C1d/C1/C42.2/C3-C1b-C3cg-C45c-C115k-C1au-C41p	0.16
T. reniformis var 1	Outdoor	D1-D4-D1ki-D1c	1.00	—	—
T. reniformis var 2	Outdoor	D1-D4-D4c-D1c-D2-D1k	0.99	C3z-C3-C3.10-C115-C3an	0.01
A. humilis var 2	Indoor	C3k/C3-C50a-C21ab-C50f-C3ba-C3dq	0.97	C1/C1c	0.03
M.capricornis var 2	Indoor	C15-C15he-C15ed-C15cq-C15vl	0.95	D1/D6-D1h-D1kg-D1ke-D1kf-D1kh	0.05
M.capricornis var 3	Indoor	C15-C15he-C15ed-C15cq-C15vl	0.98	D1/D6-D1h-D1kg-D1ke-D1kf-D1kh	0.02
T. reniformis var 2	Indoor	D1-D4-D1ki-D1c	0.97	C1/C21/C3-C1b-C1c-C42.2-C1bh	0.03

10.3389/fphys.2023.1244060

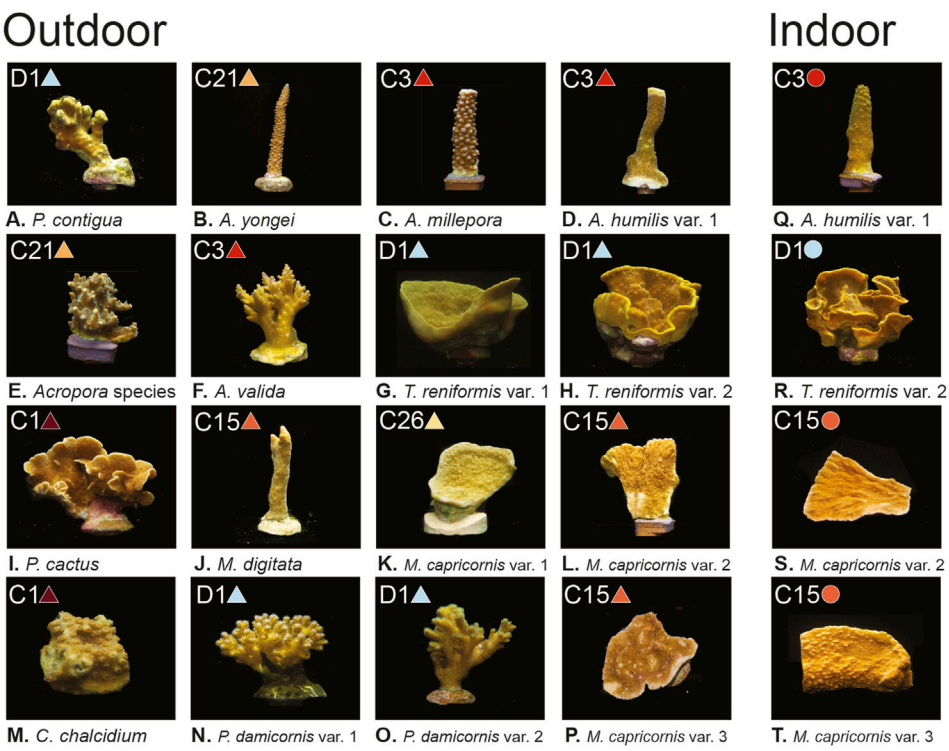

FIGURE 1
Coral images, light environments, and dominant symbiont types. **(A–T)** show the 12 coral species with one to three variants per species, separated by growth environment (Outdoor grown corals on the left and indoor grown corals on the right). Dominant symbiont type found for each coral is included in the top left of each panel, along with corresponding colored symbols (circles and triangles) which are used throughout the remaining figures to identify symbiont type. All photos taken by Audrey McQuagge.

cellular metrics and fluorescence-based phenotyping data were identified and are displayed in Figure 5.

Results

Symbiont types

Symportal analysis revealed that most corals were dominated by a single genotype (> 70% relative abundance) of Symbiodiniaceae. *Acropora* (including *A. yongei*, *A. millepora*, *A. humilis*, *A. valida*, and unknown species) predominantly hosted either *C3* or *C21* symbiont types, while *Montipora* (including *M. capricornis* and *M. digitata*) hosted primarily *C15*, but sometimes *C26*, variants (Figure 2B). The symbiont type *D1* was primarily observed in *Turbinaria*, *Psammacora*, and *Pocillopora*.

Light-response phenotype to genotype clustering and profiles

Of the 1,360 algal biometrics derived from the fluorescence-based excitation profile, 987 were found to be significantly ($p < 0.05$) different across the dominant symbiont species (*C1*, *C3*, *C15*, *C21*, *C26*, and *D1*, Table 1). These identified algal biometrics were then used to organize samples according to trait-based (light-response) phenotypes (Figure 2A), with the resulting dendrogram organized into four distinct phenotypes according to the largest clustering groups (Figure 2A). Light-response phenotype 1 contains 14 of the 15 *C15*-dominated coral colonies (*Montipora digitata* and *Montipora capricornis*), with both high and low-light acclimated fragments clustering together (Figure 2). Two additional fragments of *Acropora* sp. (*C3*) were also found in phenotype 1. Light-response phenotype 2 was predominantly (12 of 16 fragments) comprised of *Durusdinium trenchii* (*D1*)-dominated corals (low-light *T. reniformis, Pocillopora damicormis,* and *Psammacora contigua*). The remaining four coral fragments in phenotype 2, were dominated by *Cladocopium C1* (in *Cyphastrea chalcidicum* or *Pavona cactus*). Coral fragments belonging to light-response phenotype 3 were comprised of 3 *A. millepora* fragments (*C3*) and 5 fragments of high-light acclimated *Durusdinium D1*-dominated *Turbinaria renifomis*. Lastly, phenotype 4 was comprised of both high and low-light acclimated *A. humilis* (*C3*) fragments, along with all *C21* dominated corals (*A. yongei* and *Acropora* sp.), all three fragments of *M. digitata* dominated by *C26*, two fragments of *P. cactus* (*C1*) and single *C15*-dominated (*M. digitata*) and *D1*-dominated (*Turbinaria reniformis*—high light acclimated) fragments. Of the 20 coral colonies represented in this study, only four contained fragments which did not all cluster within the same phenotype. Based on row clustering and custom scripts, quantum yield of PSII (Φ_{PSII}), functional absorption cross section of PSII (σ_{PSII}), non-photochemical quenching (NPQ),

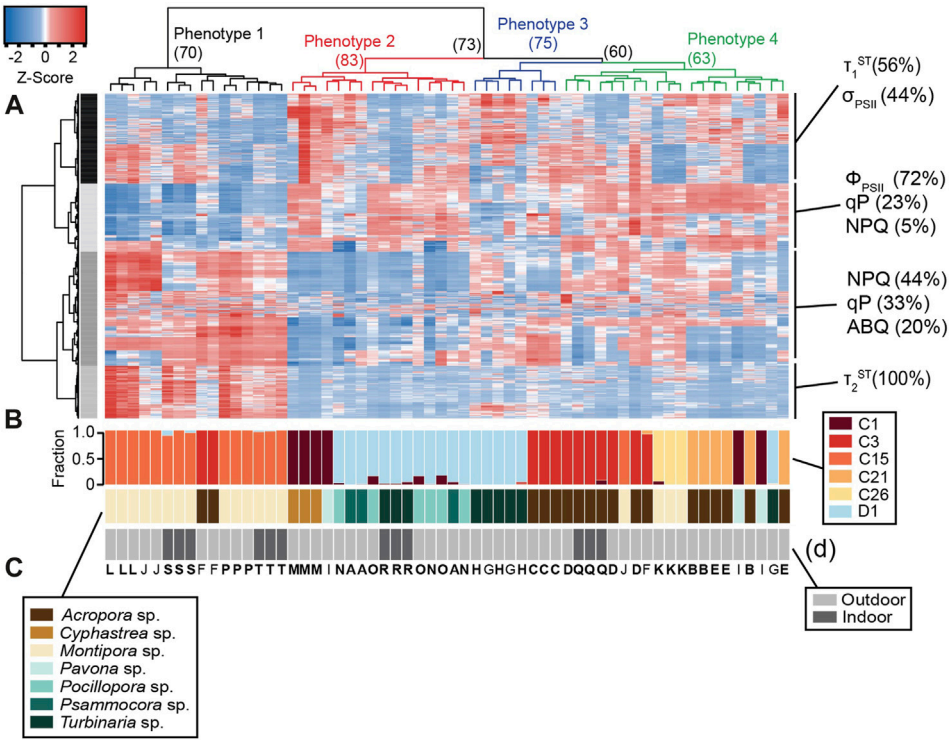

FIGURE 2
Heat map with dendrogram and relative abundance bar graphs. The heatmap **(A)** analysis reflects a total of 987 photophysiological biometrics which were found to differ significantly across symbiont types. Dominant photo-physiological metrics within each of the four identified row clusters are displayed on the right of the heatmap. The colored dendrogram above the heat reflects 4 distinct light-response phenotypes with resulting bootstrap support indicated at each major branch. The larger bar graph directly below the heat map **(B)** represents the relative abundance of symbionts within each coral sample whereas the second **(C)** and third **(D)** bar graphs represent host coral genera and coral growth environment (indoors or outdoors) respectively. Capital letters underneath the bar graphs represent the coral species listed under the various panels in Figure 1. Letters that are in bold indicate that all three fragments for that coral colony are found in the same light-response phenotype.

photochemical quenching (qP), along with the reoxidation kinetics (τ_1^{ST} and τ_2^{ST}) were determined to be the primary drivers for the observed phenotypic structure and were thus plotted in full detail (Figure 3) for each of the four light-response phenotypes described above.

A mixed linear model was used to identify spectrally dependent differences across light-response phenotypes for the photo physiological metrics, Φ_{PSII}, σ_{PSII}, NPQ, qP, τ_1^{ST}, and τ_2^{ST} reoxidation kinetics (Figure 3 and Supplementary Table S4). For all excitation wavelengths except 420 nm, phenotype 1 had significantly ($p < 0.0159$) lower Φ_{PSII} values compared to all other phenotypes. Under 420 nm excitation, Φ_{PSII} profiles for phenotype 1 were significantly ($p < 0.0001$) lower than phenotypes 2 and 4, but not phenotype 3. Additionally, Φ_{PSII} profiles for phenotype 3 were also significantly ($p < 0.001$) lower than phenotype 2 but only under 420 and 442 nm excitation whereas phenotype 3 different significantly ($p < 0.043$) from phenotype 4 under all excitation wavelengths except 525 nm. No differences across light-response phenotypes were observed for σ_{PSII} under any excitation wavelength and indicate that subtle differences may only exist when comparing across specific symbiont species (not phenotypes). Under all excitation wavelengths, nonphotochemical quenching profiles reached the highest values in phenotype 1 whereas relatively small changes were observed in phenotype 2. For phenotypes 3 and 4, NPQ values did not differ significantly from one another but represent a medium level that is significantly ($p < 0.001$) different from phenotypes 1 and 2. Photochemical quenching (qP) profiles observed in phenotypes 1 and 3 differed significantly ($p < 0.003$) from those in phenotype 2 and 4 under all excitation wavelengths. Differences in τ_1^{ST} were more sporadic across phenotypes as profiles under 420 nm excitation differed significantly ($p = 0.001$) between phenotypes 1 and 2. Under 442 nm excitation, τ_1^{ST} profiles for phenotype 1 were significantly ($p < 0.011$) different from those observed for phenotype 2 and 3. For τ_1^{ST} profiles measured under 505 nm excitation, phenotype 1 was significantly ($p < 0.021$) different from all others, while phenotypes 3 and 4 were also differed ($p < 0.027$) from one another. Lastly, τ_2^{ST} profiles for phenotype 1 had significantly ($p < 0.002$) slower (higher time constants) kinetics than those observed for all other phenotypes under all excitation wavelengths except 420 nm. Under 420 nm excitation, τ_2^{ST} profiles for phenotypes 1 and 3 were only significantly ($p < 0.002$) elevated over those found in phenotypes 2 and 4.

A mixed linear model was also used to compare spectrally dependent photo-physiological profiles within each light-response phenotype (Figure 3 and Supplementary Table S3). For Phenotype 1, Φ_{PSII}^{420} Φ_{PSII}^{442} and Φ_{PSII}^{505} profiles were significantly ($p < 0.004$) higher than Φ_{PSII}^{458} and Φ_{PSII}^{525}. For phenotype 2, Φ_{PSII}^{420}, Φ_{PSII}^{458},

10.3389/fphys.2023.1244060

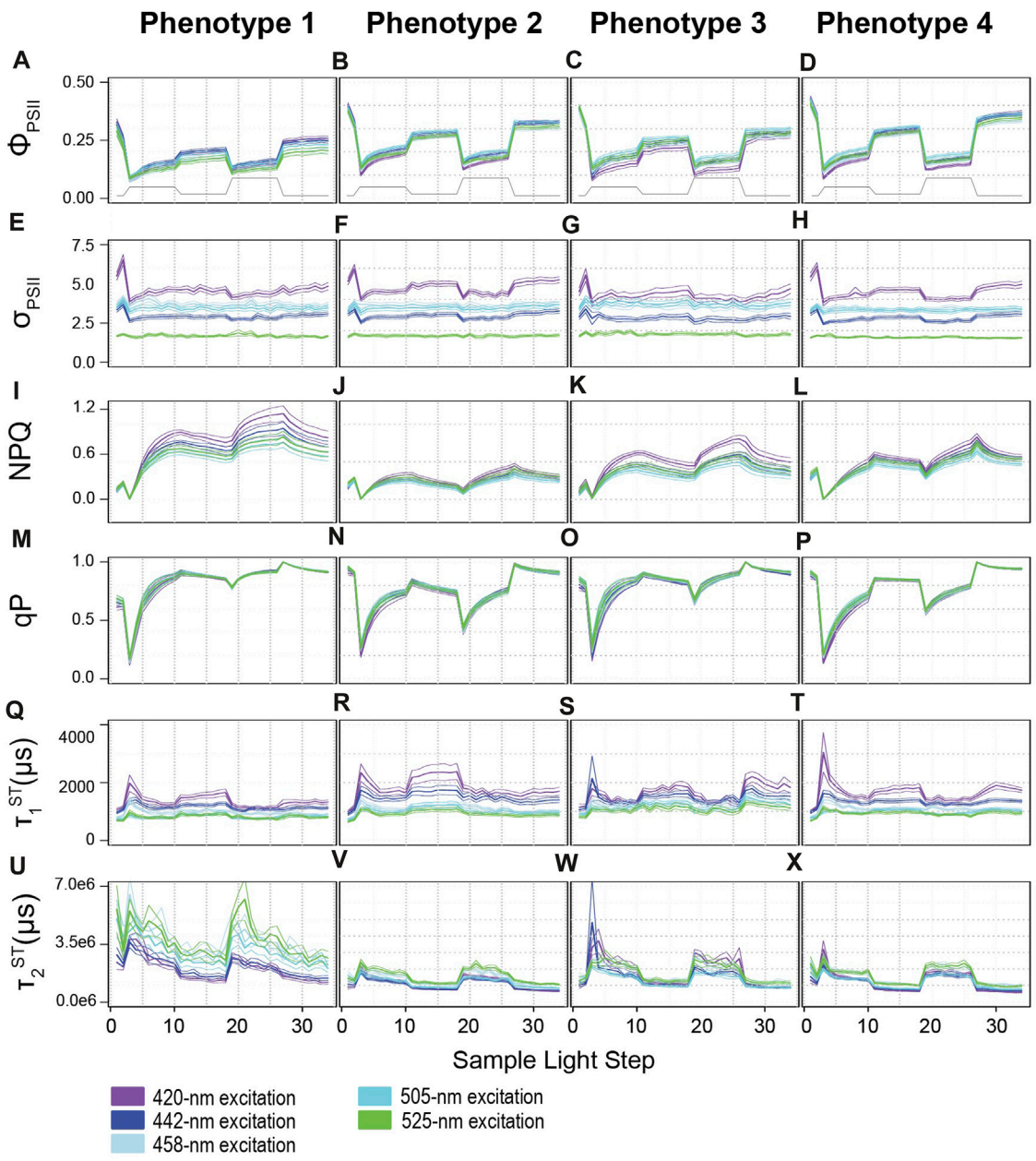

FIGURE 3
Profiles for photophysiological biometrics driving variability across light-response phenotypes. Average (± standard error) traces for photo-physiological metrics identified in Figure 2 as contributing significantly towards establishing the four phenotypes across our coral colonies. Phenotypes 1–4 are displayed from left to right. **(A–D)** reflect the Quantum Yield of PSII (Φ_{PSII}), **(E–H)** reflect the absorption cross-section of PSII (σ_{PSII}), **(I–L)** reflect non-photochemical quenching (NPQ), **(M–P)** reflect photochemical quenching (qP), **(Q–X)** reflect the reoxidation constants τ_1^{ST} and τ_2^{ST} respectively. Line color indicates excitation wavelength with purple representing 420-nm; dark blue, 442-nm; light blue, 458-nm; teal blue, 505-nm, and green, 525-nm. The grey line on panels **(A–D)** displays the variable light protocol. Bonferroni-adjusted *p*-values for comparisons across excitation wavelength and phenotype can be found in Supplementary Tables S3, S4.

and Φ_{PSII}^{525} profiles were lower ($p < 0.005$) than Φ_{PSII}^{442} and Φ_{PSII}^{505}. For phenotype 3, Φ_{PSII}^{420} appeared to be significantly ($p < 0.006$) lower than all other profiles whereas Φ_{PSII}^{505} was significantly ($p < 0.007$) higher than the rest. For phenotype 4, Φ_{PSII}^{420} and Φ_{PSII}^{458} profiles were on average lower ($p < 0.029$) than Φ_{PSII}^{442} and Φ_{PSII}^{505} profiles. For all four phenotypes, spectrally dependent σ_{PSII} differed significantly ($p < 0.021$) from one another with σ_{PSII}^{420} showing the highest and σ_{PSII}^{525} the lowest values overall. Interestingly, and in contrast to that observed for σ_{PSII}, no spectrally dependent differences in qP were observed within any phenotype. NPQ^{420} and NPQ^{442} displayed significantly ($p < 0.0001$) higher values as compared to NPQ^{458}, NPQ^{505}, and NPQ^{525} profiles within phenotype 1. For phenotype 2, NPQ^{458} profiles were similar to NPQ^{442} and NPQ^{505} whereas all others differed significantly ($p < 0.001$) from one another, as NPQ^{420} values tended to be slightly higher than the rest. For phenotypes 3 and 4, the NPQ^{420} profile

10.3389/fphys.2023.1244060

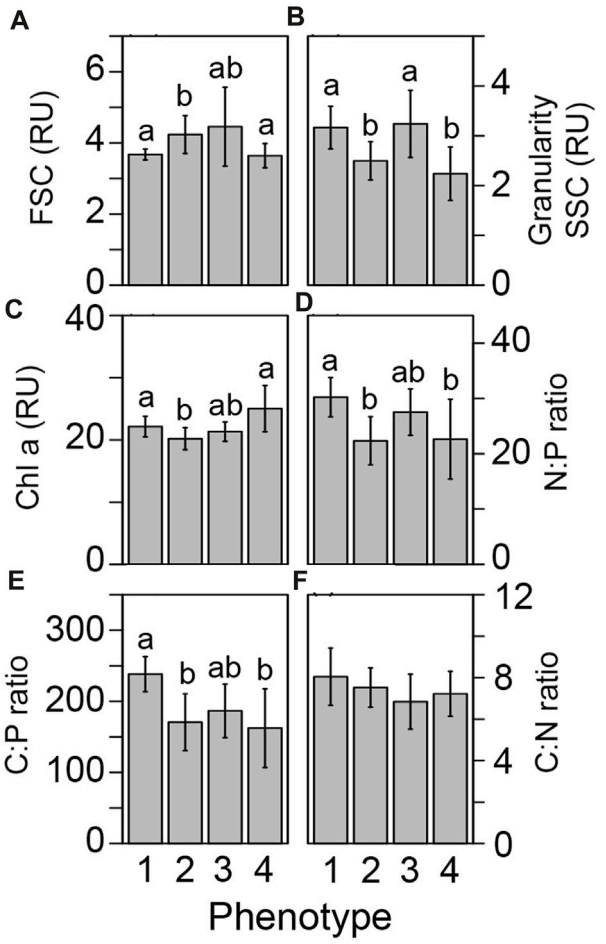

FIGURE 4
Differences in cellular physiology across light-response phenotypes. Differences in the underlying symbiont cellular physiology was compared across our four photo-physiologically derived phenotypes. Flow cytometrically derived cell size **(A)** granularity **(B)**, chlorophyll-*a* fluorescence **(C)**, Nitrogen to phosphorous **(D)**, Carbon to phosphorous **(E)**, and Carbon to nitrogen **(F)** ratios are represented as the mean (± standard error) for each phenotype. Different letters above the bars in each panel reflect significant differences (Tukey posthoc) across phenotypes.

generated significantly ($p < 0.001$) higher values whereas NPQ^{505} values were significantly ($p < 0.034$) lower than all others. All τ_1^{ST} profiles for phenotypes 2 and 3 displayed significantly different responses from one another whereas τ_1^{505} and τ_1^{525} were similar to one another within phenotypes 1 and 4. Overall, τ_1^{420} and τ_1^{442} produces slower reoxidation kinetics as compared to τ_1^{458}, τ_1^{505}, and τ_1^{525}. Lastly, τ_2^{420} and τ_2^{442} values were significantly lower than all others in phenotypes 1 and 2. For phenotype 3, τ_2^{442} and τ_2^{505} produced significantly ($p < 0.004$) lower values than τ_2^{420}, τ_2^{458}, and τ_2^{425}. In contrast, τ_2^{420}, τ_2^{442} and τ_2^{505} profiles produced significantly ($p < 0.001$) lower values than those observed for τ_2^{458}, and τ_2^{525}.

Underlying differences in cellular physiology were also compared across the four fluorescence-based light-response phenotypes (Figure 4). Cell size (FSC) was significantly ($p < 0.002$) higher in phenotype 2 as compared with phenotypes 1 and 4 (Figure 4A). Granularity (SSC) was significantly ($p < 0.008$) higher in phenotypes 2 and 4 as compared to phenotypes 1 and 3 and may indicate differences in light scattering abilities across groups (Figure 4B). Fluorescence-based chlorophyll-*a* measurements were significantly ($p < 0.025$) lower in phenotype 2 as compared with phenotypes 1 and 4 (Figure 4C). N:P and C:P ratios were significantly ($p < 0.004$) higher in phenotype 1 as compared with phenotypes 2 and 4 (Figures 4D, E).

Network analysis and correlation plots

In order to look for broad connections between primary (cellular) and secondary (photophysiological) traits, a network analysis (Figure 5) was used to search for significant correlation between each of the 1,360 fluorescence-based measurements and traditional cellular characteristics (Carbon per cell, Nitrogen per cell, Phosphate per cell, C:N ratio, N:P ratio, Cell Size, Chlorophyll-*a* (FSC), Granularity (SSC), and neutral lipids). Our analysis identified 415 correlations having a significant Pearson value of 0.6 or above. The cellular metrics N:P, C:P, and SSC displayed the greatest number of significant correlations (269, 63, and 70 respectively). For N:P ratios, the majority of positive correlations were with τ_s^{ST} measurements, while most negative correlations were with Φ_{PSII} values. For C:P ratios, most correlations occurred with NPQ or qP values while SSC correlated more broadly with various metrics including Φ_{PSII}, τ_s^{ST}, qP and connectivity. A select number of these cellular to photo-physiological correlations are displayed in full detail in Figure 6.

Discussion

Molecular and physiological techniques are commonly utilized by the coral research community to better understand what underpins genetic diversity and the broad range of environmental tolerances observed within the Symbiodiniaceae family. While the two Symbiodiniaceae genera *Cladocopium* and *Durusdinium* are separated by over 100 million years of evolutionary history (LaJeunesse et al., 2018), fluorescence-based light-response phenotypes from our analysis did not entirely converge across these broad genetic designations spread across our 12 coral colonies reared under high and low light conditions (Figure 1). For example, phenotypes 2 and 3 are comprised of corals with both symbiont genera, indicating high functional trait similarity despite large genetic differences (Figure 2A). In contrast, greater phenotypic disparity is noted across some of the five *Cladocopium* species in this study and may reflect the relatively high genetic diversity observed in this genera as compared to others (Thornhill et al., 2014; LaJeunesse et al., 2018). Indeed, host skeletal formation, tissue pigmentation and thickness, other host-regulated optical properties along with environmental parameters can all impact symbiont physiology and may lead to variability in the fluorescence-based metrics used in this study (Enriquez et al., 2005; Rodriguez-Román et al., 2006; Enríquez et al., 2017; Wangpraseurt et al., 2017a; Wangpraseurt et al., 2017b; Xiang et al., 2020; Bollati et al., 2022). Nevertheless, the degree of phenotype to genotype convergence observed within our heatmap analysis is notable, especially within the context of potentially

10.3389/fphys.2023.1244060

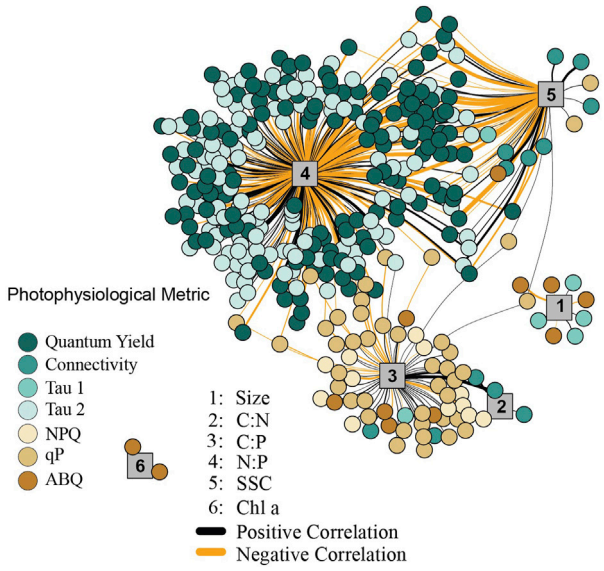

FIGURE 5
Network analysis between cellular and photophysiological traits. The network analysis only reflects significant correlations between first (cellular) and second (photo-physiological) order traits. Cellular traits are indicated by numbered grey vertices, 1 = cell size, 2 = C:N, 3 = C:P, 4 = N:P, 5 = Granularity, 6 = Chl *a*. Line thickness corresponds to the strength of the correlation (between 0.6 and 0.9 Pearson R values), with thicker lines representing traits that are more highly correlated. Positive correlations are indicated by black lines, while negative correlations are indicated by orange lines. Colored circles reflect the various photophysiological variables with strong (>0.6 Pearson R) correlation to underlying cellular metrics.

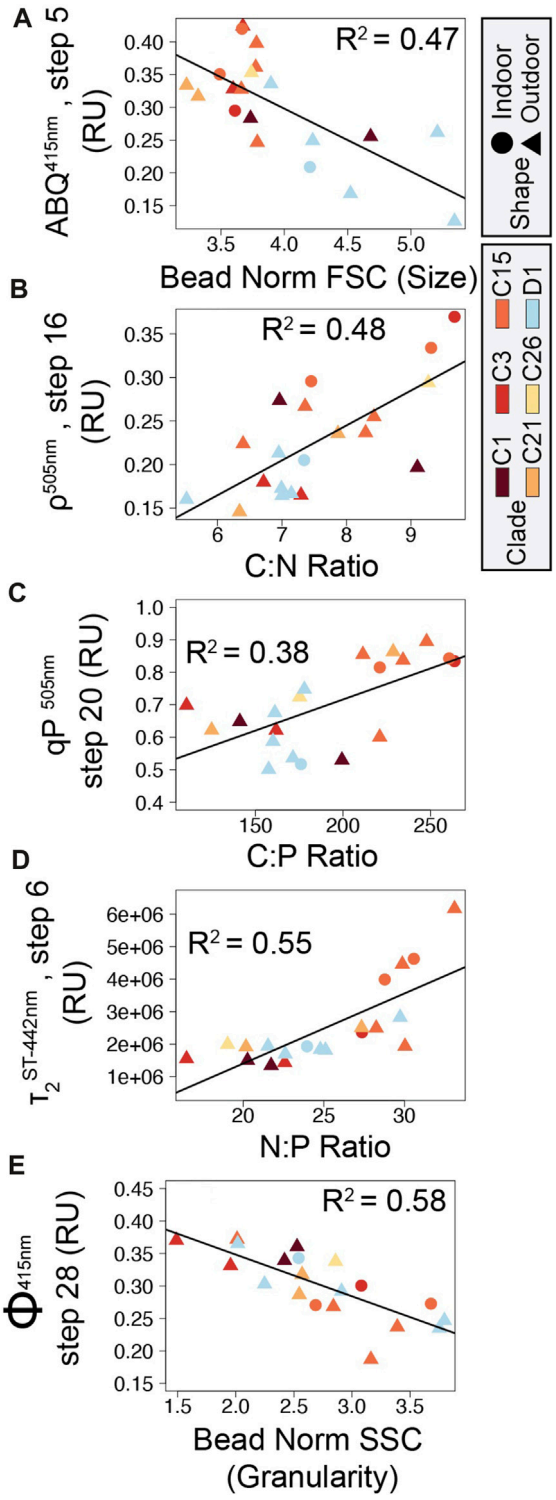

FIGURE 6
Correlation plots between symbiont cellular and photophysiological parameters. Five correlations between cellular and photo-physiological traits with high Pearson R^2 values are displayed in panels **(A)** ABQ vs. Cell size, **(B)** Connectivity vs. C:N ratio, **(C)** qP vs. C:P ratio, **(D)** τ_2^{ST} vs. N:P ratio, and **(E)** Φ_{PSII} vs. Granularity. Point shapes indicate coral growth environment (triangles: outdoor, circles: indoor) while point color indicates ITS2 symbiont type.

contributing sources of variability such as host species and light environment. High content chlorophyll-*a* fluorescence-based phenotyping is already proving useful for understanding functional trait differences and their application to ecosystem services (Suggett et al., 2022; Hoadley et al., 2023), and this study further showcases the technique's utility even across environmental light gradients while also providing direct links with underlying cellular physiology which likely regulate the observed photo physiological traits.

"High content" chlorophyl-a based phenotypes

Light acclimation state can mask species-specific differences in certain physiological metrics, as higher irradiances often lead to upregulation of stress-mitigating pathways (Ragni et al., 2010) and a reduction in photopigment production (Hoadley and Warner, 2017). This has traditionally made it difficult to capture species-specific trait-based differences without first accounting for light acclimation state. However, differences in the degree of impact that light acclimation state has on photophysiology may be largely species dependent, as high- and low-light acclimated fragments of *Cladocopium C15 and C1* (in *A. humilis*) all clustered within light-response phenotypes 1 and 4 respectively, indicating minimal impact of light acclimation state on the overall photophysiological

phenotype derived through our 'high content' chlorophyll-*a* fluorescence protocol (Figure 2). In contrast, high- and low-light acclimated *T. reniformis* coral fragments containing *Durusdinium D1* symbionts clustered into separate phenotypes, as did two of the low-light acclimated *C3*-dominated *Acropora humilis* coral fragments (Figure 2). Suggett et al., 2022 also noted that the variance in light acclimation state (light niche plasticity) differed across three different species of coral found along the same reef system and at a similar depth. Understanding how various environmental factors constrain individual coral and symbiont species combinations and their underlying phenotypes has not been feasible with industry standard fluorometers such as the diving PAM (Krämer et al., 2022). However, single-turnover fluorometers capable of measuring additional photochemical parameters are becoming increasingly popular, especially as trait-based approaches are further applied toward coral restoration and conservation practices (Voolstra et al., 2021a; Suggett et al., 2022). Still, careful consideration towards the limits of fluorescence-based measurements must still be accounted for as their utility is further explored in applied settings.

While the degree of thermal tolerance can vary across specific host/symbiont combinations (Suggett et al., 2017), comparatively high bleaching resistance in *Durusdinium D1* and *Cladocopium C15* has been a focal point of coral research (Voolstra et al., 2021b). Whether bleaching resistance is derived through similar functional traits or if mechanisms of thermal tolerance differ across the two species is currently unknown. Coral endosymbiont thermal tolerance is often linked to photochemistry (Warner et al., 1999; Fitt et al., 2001; Wang et al., 2012), yet light-response phenotypes differed across *Cladocopium C15* and *Durusdinium D1* dominated coral fragments in this study (Figures 2, 3), suggesting differences in their photosynthetic characteristics. For example, higher reliance on non-photochemical quenching (NPQ) in response to rapid changes in light is noted for the *Cladocopium C15*-dominated light-response phenotype (phenotype 1—Figure 3I) whereas *Durusdinium D1* symbionts from phenotype 2 and 3 relied more heavily on photochemical quenching to mitigate excess excitation energy as a larger proportion of PSII reaction centers remain closed throughout the actinic light protocol (Figures 3N–O). Reoxidation kinetics between the *C15* and *D1* also differed as light-response phenotype 1 had lower τ_1^{ST} values than phenotype 2 (under 420, 442, and 505 nm excitation) or 3 (under 442, 458, 505, and 525 nm excitation) and indicate faster rates of electron transport between the Q_a and Q_b sites within the PSII reaction centers of *Cladocopium C15* symbionts (Figures 3Q–S). Interestingly, faster τ_1^{ST} kinetics for C15 were coupled with much slower τ_2^{ST} rates as compared to other phenotypes (Figures 3U–W). Importantly, τ_2^{ST} values are derived from a 2 exponential equation fit model and thus do not necessarily reflect a specific rate constant (Hoadley et al., 2023), the higher values likely indicate slower rates of electron transport within and downstream of the plastoquinone pool. Alternative electron sinks or cyclic electron transport can play an important role in coping with excess excitation energy (Roberty et al., 2014; Vega de Luna et al., 2020) and differences in their utility across symbiont species may help drive the different reoxidation profiles observed here. Overall, stark contrasts in how each species copes with light energy during rapid changes in light are perhaps not surprising given the >100 million years of evolutionary history that separate the two species (LaJeunesse et al., 2018). How and if these different functional traits drive unique thermal acclimation strategies will need to be the focus of a future study.

Use of multiple LED colors to excite chlorophyll-*a* fluorescence allows for potential differences in photopigment utilization to be incorporated into our phenomic analysis. For example, spectrally-dependent variance in NPQ responses may point towards differences in how photopigments are utilized to cope with excess excitation energy within light-response phenotypes 1 and 3 (Figures 3I, K). In contrast, phenotype 2 displayed much lower levels of NPQ in response to changes in actinic light, and little spectral variance in its profile (Figure 3J). Non-photochemical quenching broadly encompasses various mechanisms utilized by photosynthetic organisms to dissipate harmful excess excitation energy absorbed by light harvesting antennae (Lacour et al., 2020). For many eukaryotic photoautotrophic taxa, the xanthophyll cycle (XC) is a major energy dissipation mechanism regulating observed changes in NPQ. While XC is not always involved in NPQ regulation, and its role in the family Symbiodiniaceae is not fully resolved, excess light energy is dissipated as heat through the inter-conversion of the photopigments (zeaxanthin to violaxanthin) or (diadinoxanthin to diatoxanthin). The sum of these various photopigments are collectively known as the xanthophyll pool, and higher concentrations are often associated with acclimation to high light (Lacour et al., 2020; Schuback et al., 2021). Importantly, these different photopigments have unique absorption spectra which may be preferentially excited by our multispectral analysis. For example, absorption spectra for extracted zeaxanthin and violaxanthin pigments indicate that both absorb light from 420, 442, and 458 nm excitation, but longer wavelength excitation (505 and 525 nm) may not be as readily absorbed by violaxanthin (Ruban et al., 2001). The spectrally-dependent variance in NPQ response observed for phenotypes 1 and 3 (Figures 3I–K) may potentially reflect differences in the relative abundance and utilization of various xanthophyll pigments. Similarly, differences in the absorption spectra between diadinoxanthin and diatoxanthin may also be present and lead to observed differences in spectrally dependent photosynthetic metrics. While additional research is needed, such a connection between XC pigment pool/utilization and excitation wavelength could provide an additional dimension for understanding NPQ responses and how they might differ across species and environmental conditions.

Significant spectrally-dependent variability is also notable within the τ_1^{ST} and τ_2^{ST} reoxidation kinetics. These time constants reflect the rate of electron transport between the Qa and Qb site of the PSII reaction center (τ_1^{ST}) and further downstream kinetics involving the PQ pool (τ_2^{ST}) and further downstream electron transport. Previous work has indeed demonstrated the utility of τ_1^{ST} for characterizing light or thermal acclimation state in reef corals (Hoadley et al., 2015; Suggett et al., 2022; Hoadley et al., 2023) or productivity rates in marine algae (Gorbunov and Falkowski, 2021). Values from τ_2^{ST} are less well understood yet the clear structure observed in our profiles

suggest this metric is indeed useful for assessing trait-based differences across species and/or environmental conditions.

Linking primary cellular traits with secondary traits (light-response photophysiology)

Underlying Symbiodiniaceae cellular physiology differed significantly across the four light-response phenotypes derived from chlorophyll-*a* fluorescence-based measurements. Linking underlying cellular physiology with more easily measured secondary traits such as photo physiology is critical for broadening the utility of multispectral and single-turnover chlorophyll-*a* fluorometers. These non-invasive, optical tools could serve as highly informative platforms for monitoring health and resilience of photosynthetic organisms, including reef corals (Suggett et al., 2022). Cellular traits, such as granularity which broadly measures the light scattering properties of a cell, were significantly higher in phenotypes 1 and 3 and may serve to deflect excess excitation energy. Reductions in photochemical quenching are more quickly relaxed in phenotypes 1 and 3 and higher granularity may serve to mitigate rapid shifts in light, functioning to reflect excess excitation energy away from the cell and reducing reliance on downstream processes such as closing PSII reaction centers in response to high light (qP, Figures 3N, P). In contrast, large cell size and lower chlorophyll content cell^{-1} for phenotype 2 could reduce light capture per cell as compared to phenotypes 1 and 2. From the cellular perspective, lower light capture by phenotype 2 maybe be beneficial for optimal performance within high-light environments, without the need to rely on secondary trait characteristics such as NPQ to mitigate excess light (Figure 3J). Indeed, cellular characteristics may help explain the photo physiological strategies employed by each phenotype. However, host skeletal and reflectance properties and their impact on the photo-symbiont's light environment and acclimation strategy need also be considered (Enriquez et al., 2005; Enríquez et al., 2017) as potential sources of variability within the chlorophyll-a fluorescent light-response phenotypes.

As chlorophyll-*a* fluorescence-based measurements are increasingly utilized for understanding photosynthetic characteristics and the utilization of stress response mechanisms by coral photosymbionts, identifying direct linkages between photo physiology and ecosystem services or underlying cellular traits are needed (Suggett et al., 2017). Our network analysis identified key correlations between basic cellular traits and photo physiological parameters across 20 different coral/symbiont combinations (Figure 5). Certain chlorophyll-*a* fluorescence-derived photophysiological parameters may serve as useful biomarkers for some primary cellular traits, especially when properly contextualized within specific environmental and/or acclimatory conditions. For example, N:P ratios are inversely correlated to quantum yield of PSII measurements and directly correlated with τ_2^{ST} reoxidation kinetics suggesting that phosphorous limited cells downregulate photochemical activity. Specifically, reductions in the quantum yield of PSII indicate reduced efficiency of light utilization for photochemistry whereas increases in τ_2^{ST} reflect slower rates of electron transport, both of which appear to occur as N:P ratios rise. From a genotype perspective, both cell size and C:P differ significantly across the predominantly *Cladocopium C15* and predominantly *Durusdinium D1* phenotypes (phenotypes 1 and 2 respectively, Figures 4A, E; Figures 6A, C). These genotype level differences in cellular physiology may also be reflected in the reoxidation kinetics values where *Durusdinium D1* (phenotype 2) appears to have slower (higher rate constant) light acclimated τ_1^{ST} (Figures 3Q, R) yet faster (lower rate constant) τ_2^{ST} (Figures 3U, V) reoxidation rates than those for *Cladocopium C15* (Figure 6D). Linking both primary and secondary trait differences, especially across species known for their thermal tolerance, can be valuable for understanding what function traits are important for establishing resilient coral symbioses.

Carbon to phosphorous ratios also appear to be correlated with various photochemical metrics, most notably photochemical and non-photochemical quenching mechanisms which function to balance light utilization within the cell. Phosphorous limitation thus appears well linked to photochemical metrics, potentially regulating gene expression along with cell ultrastructure (Ferrier-Pagès et al., 2016; Rosset et al., 2017; Lin et al., 2019). Granularity is also linked with many different photochemical metrics which is perhaps not surprising given the strong phenotype differences observed for this cellular trait (Figure 4). Overall, the strong linkages observed in our network analysis help strengthen our understanding of how differences in cellular traits across Symbiodiniaceae species regulate chlorophyll-*a* fluorescence-based phenotypes.

Conclusion

The trends in this study further emphasize the utility of using photo-physiologically derived biomarkers to generate light-response phenotypes which broadly connect to underlying coral photosymbiont cellular traits. Through the collection and analysis of large-scale chlorophyll fluorescence data sets, it is possible to resolve differences across *in hospite* coral symbionts for some species, regardless of growth environment. Further, by identifying correlations between critical first-order cellular traits and second-order photo physiological measurements, we can gain insight regarding how cellular mechanisms and characteristics affect algal photosynthesis under environmental stress. Implementation of low-cost, open-sourced methods of fluorescence measurement in coral restoration facilities may allow for quick determination of endosymbiont characteristics and better identification of the traits which underly thermal tolerance.

Data availability statement

All data needed to evaluate the conclusions in the paper are present in the paper and/or the Supplementary Materials. The raw data and analytical scripts for Figures 2–5 are available via github (khoadley/coral_phenotypes_2023) https://github.com/khoadley/coral_phenotypes_2023. Raw sequence data (fastq format) are archived via NCBI SRA (BioProject ID: PRJNA1019300) https://www.ncbi.nlm.nih.gov/bioproject/?term=PRJNA1019300.

Author contributions

AM and KH planned and designed the research. AM, BP, SL, SW, LL, and KH conducted fieldwork, and analyzed data. TM maintained the coral in healthy and stable conditions prior to and during our experiment. AM and KH wrote the manuscript. AM and KH agree to serve as corresponding authors, responsible for contact and communication. All authors contributed to the article and approved the submitted version.

Funding

The work was funded by the National Science Foundation, grant no. 2054885 to KH.

Conflict of interest

Author TM was employed by Reef Systems Coral Farm.

The remaining authors declare that the research was conducted in the absence of any commercial or financial relationships that could be construed as a potential conflict of interest.

Publisher's note

All claims expressed in this article are solely those of the authors and do not necessarily represent those of their affiliated organizations, or those of the publisher, the editors and the reviewers. Any product that may be evaluated in this article, or claim that may be made by its manufacturer, is not guaranteed or endorsed by the publisher.

Supplementary material

The Supplementary Material for this article can be found online at: https://www.frontiersin.org/articles/10.3389/fphys.2023.1244060/full#supplementary-material

References

Baker, A. C., Starger, C. J., McClanahan, T. R., and Glynn, P. W. (2004). Coral reefs: corals' adaptive response to climate change. *Nature* 430 (7001), 741. doi:10.1038/430741a

Bollati, E., Lyndby, N. H., D'Angelo, C., Kühl, M., Wiedenmann, J., Wangpraseurt, D., et al. (2022). Green fluorescent protein-like pigments optimize the internal light environment in symbiotic reef building corals. *Elife.* 11, e73521. doi:10.7554/eLife.73521

Csardi, G., and Nepusz, T. (2006). The igraph software package for complex network research. *InterJournal.* doi:10.5281/zenodo.7682609

Cunning, R., Parker, K. E., Johnson-Sapp, K., Karp, R. F., Wen, A. D., Williamson, O. M., et al. (2021). Census of heat tolerance among Florida's threatened staghorn corals finds resilient individuals throughout existing nursery populations. *Proc. R. Soc. B Biol. Sci.* 288 (1961), 20211613. doi:10.1098/rspb.2021.1613

D'Angelo, C., and Wiedenmann, J. (2014). Impacts of nutrient enrichment on coral reefs: new perspectives and implications for coastal management and reef survival. *Curr. Opin. Environ. Sustain.* 7, 82–93. doi:10.1016/j.cosust.2013.11.029

Davies, S., Gamache, M., Howe-Kerr, L., Kriefall, N., Baker, A., Banaszak, A., et al. (2022). *Building consensus around the assessment and interpretation of Symbiodiniaceae diversity*. doi:10.20944/preprints202206.0284.v1

Enriquez, S., Mendez, E. R., and Iglesias-Prieto, R. (2005). Multiple scattering on coral skeletons enhances light absorption by symbiotic algae. *Limnol. Oceanogr.* 50, 1025–1032. doi:10.4319/lo.2005.50.4.1025

Enríquez, S., Méndez, E. R., Hoegh-Guldberg, O., and Iglesias-Prieto, R. (2017). Key functional role of the optical properties of coral skeletons in coral ecology and evolution. *Proc. R. Soc. B Biol. Sci.* 284, 20161667. doi:10.1098/rspb.2016.1667

EPA (1993a). "Determination of phosphorus by semi-automated colorimetry," in *Methods for the determination of metals in environmental samples* (Elsevier), 479–495. doi:10.1016/B978-0-8155-1398-8.50027-6

EPA (1993b). "Determination of nitrate-nitrite nitrogen by automated colorimetry," in *Methods for the determination of metals in environmental samples* (Elsevier), 464–478. doi:10.1016/B978-0-8155-1398-8.50026-4

Fabricius, K. E., Mieog, J. C., Colin, P. L., Idip, D., and Van Oppen, M. J. H. (2004). Identity and diversity of coral endosymbionts (zooxanthellae) from three Palauan reefs with contrasting bleaching, temperature and shading histories. *Mol. Ecol.* 13 (8), 2445–2458. doi:10.1111/j.1365-294X.2004.02230.x

Ferrier-Pagès, C., Godinot, C., D'Angelo, C., Wiedenmann, J., and Grover, R. (2016). Phosphorus metabolism of reef organisms with algal symbionts. *Ecol. Monogr.* 86 (3), 262–277. doi:10.1002/ecm.1217

Fitt, W., Brown, B., Warner, M., and Dunne, R. (2001). Coral bleaching: interpretation of thermal tolerance limits and thermal thresholds in tropical corals. *Coral Reefs* 20 (1), 51–65. doi:10.1007/s003380100146

Galili, T. (2015). dendextend: an R package for visualizing, adjusting, and comparing trees of hierarchical clustering. *Bioinformatics* 31, 3718–3720. doi:10.1093/bioinformatics/btv428

Gorbunov, M. Y., and Falkowski, P. G. (2021). Using chlorophyll fluorescence kinetics to determine photosynthesis in aquatic ecosystems. *Limnol. Oceanogr.* 66 (1), 1–13. doi:10.1002/lno.11581

Goyen, S., Pernice, M., Szabó, M., Warner, M. E., Ralph, P. J., and Suggett, D. J. (2017). A molecular physiology basis for functional diversity of hydrogen peroxide production amongst Symbiodinium spp. (Dinophyceae). *Mar. Biol.* 164 (3), 46. doi:10.1007/s00227-017-3073-5

Hoadley, K. D., and Warner, M. E. (2017). Use of open source hardware and software platforms to quantify spectrally dependent differences in photochemical efficiency and functional absorption cross section within the dinoflagellate symbiodinium spp. *Front. Mar. Sci.* 4, 365. doi:10.3389/fmars.2017.00365

Hoadley, K. D., Pettay, D. T., Grottoli, A. G., Cai, W.-J., Melman, T. F., Schoepf, V., et al. (2015). Physiological response to elevated temperature and pCO2 varies across four pacific coral species: understanding the unique host+symbiont response. *Sci. Rep.* 5 (1), 18371. doi:10.1038/srep18371

Hoadley, K. D., Pettay, D. T., Lewis, A., Wham, D., Grasso, C., Smith, R., et al. (2021). Different functional traits among closely related algal symbionts dictate stress endurance for vital Indo-Pacific reef-building corals. *Glob. Change Biol.* 27 (20), 5295–5309. doi:10.1111/gcb.15799

Hoadley, K. D., Lockridge, G., McQuagge, A., Pahl, B., Lowry, S., Wong, S., et al. (2023). A phenomic modeling approach for using chlorophyll-a fluorescence-based measurements on coral photosymbionts: A step towards bio-optical bleaching prediction. *Front. Mar. Sci.* 10. doi:10.3389/fmars.2023.1092202

Hoegh-Guldberg, O., and Smith, G. J. (1989). The effect of sudden changes in temperature, light and salinity on the population density and export of zooxanthellae from the reef corals *Stylophora pistillata Esper* and *Seriatopora hystrix Dana*. *J. Exp. Mar. Biol. Ecol.* 129 (3), 279–303. doi:10.1016/0022-0981(89)90109-3

Hothorn, T., Bretz, F., and Westfall, P. (2008). Simultaneous inference in general parametric models. *Biometrical J.* 50 (3), 346–363. doi:10.1002/bimj.200810425

Hume, B. C. C., Smith, E. G., Ziegler, M., Warrington, H. J. M., Burt, J. A., LaJeunesse, T. C., et al. (2019). SymPortal: A novel analytical framework and platform for coral algal symbiont next-generation sequencing *ITS2* profiling. *Mol. Ecol. Resour.* 19 (4), 1063–1080. doi:10.1111/1755-0998.13004

Johannes, R. E., and Wiebe, W. J. (1970). Method for determination of coral tissue biomass and composition. *Limnol. Oceanogr.* 15, 822–824. doi:10.4319/lo.1970.15.5.0822

Kolber, Z. S., Prášil, O., and Falkowski, P. G. (1998). Measurements of variable chlorophyll fluorescence using fast repetition rate techniques: defining methodology and experimental protocols. *Biochimica Biophysica Acta (BBA) - Bioenergetics* 1367 (1), 88–106. doi:10.1016/S0005-2728(98)00135-2

Krämer, W. E., Iglesias-Prieto, R., and Enríquez, S. (2022). Evaluation of the current understanding of the impact of climate change on coral physiology after three decades of experimental research. *Communications Biology*. 5, 1418. doi:10.1038/s42003-022-04353-1

Krueger, T., and Gates, R. D. (2012). Cultivating endosymbionts—host environmental mimics support the survival of *symbiodinium* C15 ex hospite. *J. Exp. Mar. Biol. Ecol.* 413, 169–176. doi:10.1016/j.jembe.2011.12.002

Kuznetsova, A., Brockhoff, P. B., and Christensen, R. H. B. (2017). lmerTest package: tests in linear mixed effects models. *J. Stat. Softw.* 82 (13), 1–26. doi:10.18637/jss.v082.i13

Lacour, T., Babin, M., and Lavaud, J. (2020). Diversity in xanthophyll cycle pigments content and related nonphotochemical quenching (NPQ) among microalgae: implications for growth strategy and ecology. *J. Phycol.* 56 (2), 245–263. doi:10.1111/jpy.12944

LaJeunesse, T. C., and Thornhill, D. J. (2011). Improved resolution of reef-coral endosymbiont (symbiodinium) species diversity, ecology, and evolution through psbA non-coding region genotyping. *PLoS ONE* 6 (12), e29013. doi:10.1371/journal.pone.0029013

LaJeunesse, T. C., Loh, W. K. W., van Woesik, R., Hoegh-Guldberg, O., Schmidt, G. W., and Fitt, W. K. (2003). Low symbiont diversity in southern Great Barrier Reef corals, relative to those of the Caribbean. *Limnol. Oceanogr.* 48 (5), 2046–2054. doi:10.4319/lo.2003.48.5.2046

LaJeunesse, T. C., Parkinson, J. E., Gabrielson, P. W., Jeong, H. J., Reimer, J. D., Voolstra, C. R., et al. (2018). Systematic revision of *Symbiodiniaceae* highlights the antiquity and diversity of coral endosymbionts. *Curr. Biol.* 28 (16), 2570–2580. doi:10.1016/j.cub.2018.07.008

LaJeunesse, T. (2002). Diversity and community structure of symbiotic dinoflagellates from Caribbean coral reefs. *Mar. Biol.* 141 (2), 387–400. doi:10.1007/s00227-002-0829-2

Lewis, A., Chan, A., and LaJeunesse, T. (2018). New species of closely related endosymbiotic dinoflagellates in the greater caribbean have niches corresponding to host coral phylogeny. *J. Eukaryot. Microbiol.* 66, 469–482. doi:10.1111/jeu.12692

Lin, S., Yu, L., and Zhang, H. (2019). Transcriptomic responses to thermal stress and varied phosphorus conditions in fugacium kawagutii. *Microorganisms* 7 (4), 96. doi:10.3390/microorganisms7040096

Loeblich, A. R., and Sherley, J. L. (1979). Observations on the theca of the motile phase of free-living and symbiotic isolates of Zooxanthella microadriatica (Freudenthal) comb.nov. *J. Mar. Biol. Assoc. U. K.* 59 (1), 195–205. Cambridge Core. doi:10.1017/S0025315400046270

Mansour, J. S., Pollock, F. J., Díaz-Almeyda, E., Iglesias-Prieto, R., and Medina, M. (2018). Intra- and interspecific variation and phenotypic plasticity in thylakoid membrane properties across two *Symbiodinium* clades. *Coral Reefs* 37 (3), 841–850. doi:10.1007/s00338-018-1710-1

McIlroy, S. E., Wong, J. C. Y., and Baker, D. M. (2020). Competitive traits of coral symbionts may alter the structure and function of the microbiome. *ISME J.* 14 (10), 2424–2432. doi:10.1038/s41396-020-0697-0

Muscatine, L., and Hand, C. (1958). Direct evidence for the transfer of materials from symbiotic algae to the tissues of a coelenterate. *Proc. Natl. Acad. Sci.* 44 (12), 1259–1263. doi:10.1073/pnas.44.12.1259

Pasaribu, B., Li, Y.-S., Kuo, P.-C., Lin, I.-P., Tew, K. S., Tzen, J. T. C., et al. (2016). The effect of temperature and nitrogen deprivation on cell morphology and physiology of *Symbiodinium*. *Oceanologia* 58 (4), 272–278. doi:10.1016/j.oceano.2016.04.006

Pettay, D. T., Wham, D. C., Smith, R. T., Iglesias-Prieto, R., and LaJeunesse, T. C. (2015). Microbial invasion of the Caribbean by an Indo-Pacific coral zooxanthella. *Proc. Natl. Acad. Sci.* 112 (24), 7513–7518. doi:10.1073/pnas.1502283112

Ragni, M., Airs, R. L., Hennige, S. J., Suggett, D. J., Warner, M. E., and Geider, R. J. (2010). PSII photoinhibition and photorepair in Symbiodinium (Pyrrhophyta) differs between thermally tolerant and sensitive phylotypes. *Mar. Ecol. Prog. Ser.* 406, 57–70. doi:10.3354/meps08571

Roberty, S., Bailleul, B., Berne, N., Franck, F., and Cardol, P. (2014). PSI Mehler reaction is the main alternative photosynthetic electron pathway in Symbiodinium sp., symbiotic dinoflagellates of cnidarians. *New Phytologist* 204 (1), 81–91. doi:10.1111/nph.12903

Rodríguez-Román, A., Hernández-Pech, X., Thome, E., Enríquez, S., and Iglesias-Prieto, R. (2006). Photosynthesis and light utilization in the Caribbean coral Montastraea faveolata recovering from a bleaching event. *Limnol. Oceanogr.* 51 (6), 2702–2710. doi:10.4319/lo.2006.51.6.2702

Rosset, S., Wiedenmann, J., Reed, A. J., and D'Angelo, C. (2017). Phosphate deficiency promotes coral bleaching and is reflected by the ultrastructure of symbiotic dinoflagellates. *Mar. Pollut. Bull.* 118 (1-2), 180–187. doi:10.1016/j.marpolbul.2017.02.044

Ruban, A. V., Pascal, A. A., Robert, B., and Horton, P. (2001). Configuration and dynamics of xanthophylls in light-harvesting antennae of higher plants. Spectroscopic analysis of isolated light-harvesting complex of photosystem II and thylakoid membranes. *J. Biol. Chem.* 276 (27), 24862–24870. doi:10.1074/jbc.M103263200

Saad, O. S., Lin, X., Ng, T. Y., Li, L., Ang, P., and Lin, S. (2020). Genome size, rDNA copy, and qPCR assays for Symbiodiniaceae. *Front. Microbiol.* 11, 847. doi:10.3389/fmicb.2020.00847

Sampayo, E. M., Ridgway, T., Bongaerts, P., and Hoegh-Guldberg, O. (2008). Bleaching susceptibility and mortality of corals are determined by fine-scale differences in symbiont type. *Proc. Natl. Acad. Sci.* 105 (30), 10444–10449. doi:10.1073/pnas.0708049105

Scheufen, T., Iglesias-Prieto, R., and Enríquez, S. (2017). Changes in the number of symbionts and *symbiodinium* cell pigmentation modulate differentially coral light absorption and photosynthetic performance. *Front. Mar. Sci.* 4, 309. doi:10.3389/fmars.2017.00309

Schuback, N., Tortell, P. D., Berman-Frank, I., Campbell, D. A., Ciotti, A., Courtecuisse, E., et al. (2021). Single-turnover variable chlorophyll fluorescence as a tool for assessing phytoplankton photosynthesis and primary productivity: opportunities, caveats and recommendations. *Front. Mar. Sci.* 8, 690607. doi:10.3389/fmars.2021.690607

Sheffield, V. C., Cox, D. R., Lerman, L. S., and Myers, R. M. (1989). Attachment of a 40-base-pair G + C-rich sequence (GC-clamp) to genomic DNA fragments by the polymerase chain reaction results in improved detection of single-base changes. *Proc. Natl. Acad. Sci.* 86 (1), 232–236. doi:10.1073/pnas.86.1.232

Steen, R. G., and Muscatine, L. (1987). Low temperature evokes rapid exocytosis of symbiotic algae by a sea anemone. *Biol. Bull.* 172 (2), 246–263. doi:10.2307/1541797

Suggett, D. J., Goyen, S., Evenhuis, C., Szabó, M., Pettay, D. T., Warner, M. E., et al. (2015). Functional diversity of photobiological traits within the genus *Symbiodinium* appears to be governed by the interaction of cell size with cladal designation. *New Phytol.* 208 (2), 370–381. doi:10.1111/nph.13483

Suggett, D. J., Warner, M. E., and Leggat, W. (2017). Symbiotic dinoflagellate functional diversity mediates coral survival under ecological crisis. *Trends Ecol. Evol.* 32 (10), 735–745. doi:10.1016/j.tree.2017.07.013

Suggett, D. J., Nitschke, M., Hughes, D., Bartels, N., Camp, E., Dilernia, N., et al. (2022). Toward bio-optical phenotyping of reef-forming corals using Light-Induced Fluorescence Transient-Fast Repetition Rate fluorometry. *Limnol. Oceanogr. Methods* 20, 172–191. doi:10.1002/lom3.10479

Sully, S., and van Woesik, R. (2020). Turbid reefs moderate coral bleaching under climate-related temperature stress. *Glob. Change Biol.* 26 (3), 1367–1373. doi:10.1111/gcb.14948

Suzuki, R., and Shimodaira, H. (2006). Pvclust: an R package for assessing the uncertainty in hierarchical clustering. *Bioinformatics* 22 (12), 1540–1542. doi:10.1093/bioinformatics/btl117

Szabó, M., Wangpraseurt, D., Tamburic, B., Larkum, A. W. D., Schreiber, U., Suggett, D. J., et al. (2014). Effective light absorption and absolute electron transport rates in the coral Pocillopora damicornis. *Plant Physiology Biochem.* 83, 159–167. doi:10.1016/j.plaphy.2014.07.015

Takabayashi, M., Adams, L. M., Pochon, X., and Gates, R. D. (2012). Genetic diversity of free-living *Symbiodinium* in surface water and sediment of Hawai'i and Florida. *Coral Reefs* 31 (1), 157–167. doi:10.1007/s00338-011-0832-5

Tchernov, D., Kvitt, H., Haramaty, L., Bibby, T. S., Gorbunov, M. Y., Rosenfeld, H., et al. (2011). Apoptosis and the selective survival of host animals following thermal bleaching in zooxanthellate corals. *Proc. Natl. Acad. Sci.* 108 (24), 9905–9909. doi:10.1073/pnas.1106924108

Thornhill, D. J., Lewis, A. M., Wham, D. C., and LaJeunesse, T. C. (2014). Host-specialist lineages dominate the adaptive radiation of reef coral endosymbionts. *Evolution* 68 (2), 352–367. doi:10.1111/evo.12270

Vega de Luna, F., Córdoba-Granados, J. J., Dang, K.-V., Roberty, S., and Cardol, P. (2020). *In vivo* assessment of mitochondrial respiratory alternative oxidase activity and cyclic electron flow around photosystem I on small coral fragments. *Sci. Rep.* 10 (1), 17514. doi:10.1038/s41598-020-74557-0

Voolstra, C. R., Valenzuela, J. J., Turkarslan, S., Cárdenas, A., Hume, B. C. C., Perna, G., et al. (2021a). Contrasting heat stress response patterns of coral holobionts across the Red Sea suggest distinct mechanisms of thermal tolerance. *Mol. Ecol.* 30 (18), 4466–4480. doi:10.1111/mec.16064

Voolstra, C. R., Suggett, D. J., Peixoto, R. S., Parkinson, J. E., Quigley, K. M., Silveira, C. B., et al. (2021b). Extending the natural adaptive capacity of coral holobionts. *Nat. Rev. Earth Environ.* 2 (11), 747–762. doi:10.1038/s43017-021-00214-3

Wang, J. T., Meng, P. J., Chen, Y. Y., and Chen, C. A. (2012). Determination of the thermal tolerance of Symbiodinium using the activation energy for inhibiting photosystem II activity. *Zool. Stud.* 51, 137–142.

Wangpraseurt, D., Holm, J. B., Larkum, A. W. D., Pernice, M., Ralph, P. J., and Suggett, D. J. (2017a). *In vivo* microscale measurements of light and photosynthesis during coral bleaching: evidence for the optical feedback loop. *Frontiers in microbiology.* 8, 59. doi:10.3389/fmicb.2017.00059

Wangpraseurt, D., Wentzel, C., Jacques, S. L., Wagner, M., and Kühl, M. (2017b). *In vivo* imaging of coral tissue and skeleton with optical coherence tomography. *Journal of The Royal Society Interface.* 14, 20161003. doi:10.1098/rsif.2016.1003

Warner, M., and Suggett, D. (2016). "The photobiology of symbiodinium spp.: linking physiological diversity to the implications of stress and resilience," in *The Cnidaria, past, present and future*, 489–509. doi:10.1007/978-3-319-31305-4_30

Warner, M. E., Fitt, W. K., and Schmidt, G. W. (1999). Damage to photosystem II in symbiotic dinoflagellates: A determinant of coral bleaching. *Proc. Natl. Acad. Sci.* 96 (14), 8007–8012. doi:10.1073/pnas.96.14.8007

Wiedenmann, J., D'Angelo, C., Smith, E. G., Hunt, A. N., Legiret, F.-E., Postle, A. D., et al. (2012). Nutrient enrichment can increase the susceptibility of reef corals to bleaching. *Nat. Clim. Change* 3 (2), 160–164. doi:10.1038/nclimate1661

Xiang, T., Lehnert, E., Jinkerson, R. E., Clowez, S., Kim, R. G., and DeNofrio, J. C. (2020). Symbiont population control by host-symbiont metabolic interaction in Symbiodiniaceae-cnidarian associations. *Nature communications.* 11 (9), 1–9. doi:10.1038/s41467-019-13963-z

Yellowlees, D., Rees, T. A. V., and Leggat, W. (2008). Metabolic interactions between algal symbionts and invertebrate hosts. *Plant, Cell. and Environ.* 31 (5), 679–694. doi:10.1111/j.1365-3040.2008.01802.x